Int. J. Appl. Math. Comput. Sci., 2024, Vol. 34, No. 3, 409–423
DOI: 10.61822/amcs-2024-0029

DEVELOPMENT OF A GUARANTEED MINIMUM DETECTABLE SENSOR FAULT DIAGNOSIS SCHEME

MARCIN WITCZAK [a], MARCIN PAZERA [a,*], PAWEŁ MAJDZIK [a], RYSZARD MATYSIAK [b]

[a]Institute of Control and Computation Engineering
University of Zielona Góra
ul. prof. Z. Szafrana 2, 65-516 Zielona Góra, Poland
e-mail: {m.witczak,m.pazera,p.majdzik}@issi.uz.zgora.pl

[b]Institute of Mechanical Engineering
University of Zielona Góra
ul. prof. Z. Szafrana 4, 65-516 Zielona Góra, Poland
e-mail: r.matysiak@iibnp.uz.zgora.pl

The paper deals with the estimation of sensor faults for dynamic systems as well as the assessment of the uncertainty of the resulting estimates. For that purpose, it is assumed that the external disturbances are bounded within an ellipsoidal domain. This allows considering both stochastic and deterministic process and measurement uncertainties. Under such an assumption, a fault diagnosis scheme is developed with a prescribed convergence rate and accuracy. To achieve fault estimation, a conversion into an equivalent descriptor system is utilized. The paper provides a full stability and convergence analysis of the estimator including observability analysis. As a result, a set of complementary fault uncertainty intervals is obtained, which are minimized in such a way as to obtain a minimum detectable sensor fault. The final part of the paper exhibits a numerical example concerning fault estimation of a multi-tank system. The obtained results clearly confirm the performance of the proposed estimator expressed in the minimum detectable fault intervals.

Keywords: minimum detectable fault, fault estimation, fault diagnosis, sensor fault.

1. Introduction

Owing to the intense development of the industrial Internet of things (IIoT) (Witczak *et al.*, 2023) towards Industry 4.0, companies are increasing the number of sensors and actuators that cover the existing and newly developed infrastructures. This leads to a higher probability of faults. Indeed, the more sensor/actuators, the larger a chance that some of them can be faulty. Undoubtedly, a fault may impair the overall system performance, and hence it may also lead to its failure. This brings us to a straightforward conclusion that faults should be detected as fast as possible taking into account disturbances, model uncertainties, etc. Undeniably, these unappealing factors may hide the effect of the fault. Thus, the main objective of this paper is to answer the question: What is the smallest possible sensor fault which can be detected for a given class of dynamic systems?

The answer to this nontrivial issue contributes directly to preventing a reduction of the system's availability and productivity. Indeed, the sooner a fault is detected, the sooner a recovery or repair action can be performed. This is the reason why fault diagnosis (FD) plays an important role in safety and reliability of complex systems (Blanke *et al.*, 2006; Patton and Chen, 1997; Zhang and Jiang, 2008).

Many successful techniques are now used in FD research (Rodrigues *et al.*, 2015; Pazera and Witczak, 2019; Samada *et al.*, 2022; Zhirabok and Shumsky, 2018). FD is primarily focused on fault detection and isolation (FDI) (Yang *et al.*, 2015; Jung and Frisk, 2018). However, with the development of fault-tolerant control (FTC) (Pizzi *et al.*, 2019; Pazera *et al.*, 2018; Bounemeur *et al.*, 2018; Chen *et al.*, 2018; Kukurowski *et al.*, 2022), fault estimation has become an important research area in modern FD (Chen *et al.*, 2018; Wen *et al.*, 2022; Ye *et al.*, 2016). Fault estimation provides information

*Corresponding author

about the presence, location and size of a fault. Such information is necessary to accommodate the fault by means of appropriate FTC methods (Rotondo *et al*., 2015; Liu *et al*., 2018) or simply a hardware replacement.

There are many fault estimation schemes using observer-based approaches (Zhang *et al*., 2018; Rinaldi *et al*., 2018; Peng *et al*., 2019). Zhang *et al*. (2018) reviewed observer-based fault estimation techniques for various classes of systems, including continuous-time, discrete-time and fuzzy systems. For example, Rinaldi *et al*. (2018) provide a novel estimation scheme for power grids based on distributed observers, i.e., the distributed observers use only knowledge of local system information. A nonlinear observer for the estimation of vehicle speed along with the tire-road friction factor was designed by Peng *et al*. (2019). Nasrolahi and Abdollahi (2018) address an integrated sensor fault detection and recovery for a satellite attitude control system. The developed nonlinear observer allows detecting faults both in angular rate and attitude sensors simultaneously. Gupta *et al*. (2017) considered the problem of chaotic system synchronisation for secure communication. This solution was based on the observer design approach. The paper by Chandra *et al*. (2015) concerns the synchronization of a chaotic and Rossler system in a finite-time for safe communication, and in that of Gupta *et al*. (2017) the Lorenz system was applied for the transmission of a signal for secure communication. Boutayeb *et al*. (2002) and Wang *et al*. (2009) present a novel technique for both synchronization and secure communication of chaotic systems (well-known chaotic Lorentz systems). In the work of Boutayeb *et al*. (2002), the proposed approach is based on generalized state space observer design. Wang *et al*. (2009), proposed a descriptor observer that ensures accurate estimation of both the system states and the transmitted signals. Dimassi *et al*. (2012) present new unknown-input observers for secured transmission of information based on master–slave synchronization.

As already mentioned, the present paper proposes a method for determining a minimum detectable sensor fault (MDF) for a class of linear dynamic systems along with assessing the uncertainty of the resulting estimates. The proposed MDF approach is based on a set of complementary fault uncertainty intervals, which are minimized to obtain a minimum detectable sensor fault. The minimum detectable fault is often used as an index to assess and characterise the performance of fault detection. It also describes the sensitivity of FD. The reference literature covering the MDF provides many different points of view. In the work of Wang *et al*. (2022), the sensor fault detection problem in a dynamic point-the-bit rotary steerable system was considered. The authors proposed a finite-frequency fault detection observer and the calculation method of minimum detectable faults. Xu (2022) designed a framework for computing minimal detectable and isolable faults of set-based active fault diagnosis methods for discrete-time linear time-invariant systems. The guaranteed minimal detectable and isolable faults were computed by solving a mixed integer quadratic fractional programming problem. In the work of Tan *et al*. (2023), a confidence set-based computational method of minimal detectable faults was presented. The proposed method was based on the confidence set-separation condition between healthy and faulty residual sets for discrete linear time-invariant systems. Mustafa *et al*. (2016) proposed an SMI technique. It is also based on minimum identified uncertainty bounds violation. Such a methodology relies on the set membership identification (SMI) technique. Minimal detectable faults for actuators and sensors were obtained by solving a nonconvex optimization problem. Furthermore, Samada *et al*. (2022) analyses the problem of robust fault detection considering parametric uncertainty with zonotopes. A zonotopic recursive least squares estimator is proposed, which takes as a reference the minimum detectable fault generated in the worst case. In the work of Kodakkadan *et al*. (2017), a detectable sensor fault obtained with interval observers was considered. Minimum detectable sensor faults are analyzed by means of both invariant-sets and classical fault-sensitivity method. A framework for computing the MDF by constructing a minimal robust positively invariant set of linear parameter varying systems based on a poly-quadratic Lyapunov function was proposed by Tan *et al*. (2019).

The main contribution of this paper is to propose a fault estimator with a possibly small uncertainty under a given feasible ellipsoidal set of unknown exogenous disturbances. Unlike the approaches presented in the literature, the proposed solution focuses on a single sensor fault. This means that a coverage of all sensor faults is possible by using a bank of such estimators, which is presented in Fig. 1. The above strategy is motivated by the fact that it is impossible to obtain a single sensor fault estimator which will provide the same estimation quality for all n_s sensor faults. This simply means that each estimator (in the bank of n_s of them) estimates all faults but is designed in such a way as to provide an estimate of the i-th ($i = 1, \ldots, n_s$) fault with as little uncertainty as possible. The main advantage of the proposed approach is that the minimum value of the estimation uncertainty is achieved and expressed by an uncertainty interval. This, in turn, gives us the value of the minimum detectable fault, i.e., a fault which can be distinguished from the external disturbances and the remaining uncertainties. The MDF pertains to sensor faults and it is absolutely important due to the fact that it allows process engineers to notice early fault occurrence. This is particularly important because it gives them more time to react to such a fault in order to minimize its effects in time and prevent a failure that may have serious consequences. In consequence, it is

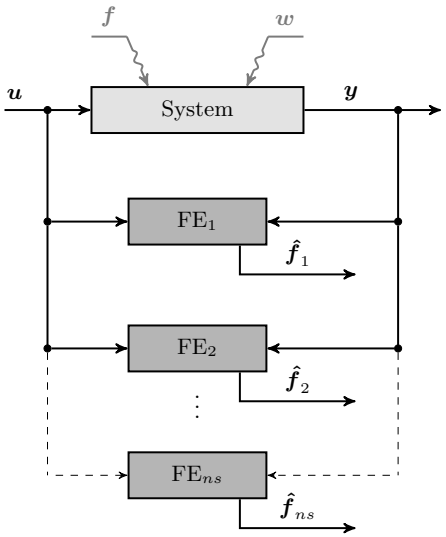

Fig. 1. Bank of sensor fault estimators.

important to notice a fault occurrence at its minimum level, which allows, e.g., safe operation and minimizes the costs of further maintenance. Moreover, in some way the MDF prevents false alarms due to the bounds which ensure that the fault is always inside them. Finally, the convergence as well as stability analysis pertaining to the MDF is provided as well.

The paper is structured as follows. In Section 2, the problem is introduced and essential preliminary information is presented. Section 3 outlines a new estimator structure along with the underlying convergence conditions. Section 4 expands the proposed strategy by incorporating a design strategy towards a minimum detectable fault. An illustrative example is then provided in Section 5. Finally, the paper is concluded in Section 6.

2. Preliminaries

Let us start with defining a linear dynamic system, which will be the subject of the discussion presented in the framework of this paper:

$$\bar{\boldsymbol{x}}_{k+1} = \bar{\boldsymbol{A}}\bar{\boldsymbol{x}}_k + \bar{\boldsymbol{B}}\boldsymbol{u}_k + \bar{\boldsymbol{W}}_1\boldsymbol{w}_{1,k}, \tag{1}$$

$$\boldsymbol{y}_k = \bar{\boldsymbol{C}}\bar{\boldsymbol{x}}_k + \boldsymbol{C}_f\boldsymbol{f}_k + \bar{\boldsymbol{W}}_2\boldsymbol{w}_{2,k}, \tag{2}$$

where $\bar{\boldsymbol{x}}_k \in \mathbb{X} \subset \mathbb{R}^n$, $\boldsymbol{u}_k \in \mathbb{R}^r$, $\boldsymbol{y}_k \in \mathbb{R}^m$, are the state, control input and output vectors, whilst $\boldsymbol{f}_k \in \mathbb{F}_s \subset \mathbb{R}^s$ is the sensor fault. Moreover, $\boldsymbol{w}_{1,k} \in \mathbb{R}^{n_{w1}}$ and $\boldsymbol{w}_{2,k} \in \mathbb{R}^{n_{w2}}$ are unknown exogenous external disturbances affecting the process and output measurements, respectively. Note also that $\boldsymbol{C}_f$ is a fault distribution matrix satisfying $\text{rank}(\boldsymbol{C}_f) = s$. This matrix is typically formed with an appropriate subset of the columns of the identity matrix $\boldsymbol{I}_m$. Subsequently, the system (1)–(2) is converted into an equivalent form,

$$\boldsymbol{E}\boldsymbol{x}_{k+1} = \boldsymbol{A}\boldsymbol{x}_k + \boldsymbol{B}\boldsymbol{u}_k + \boldsymbol{W}_1\boldsymbol{w}_{1,k}, \tag{3}$$

$$\boldsymbol{y}_k = \boldsymbol{C}\boldsymbol{x}_k + \boldsymbol{W}_2\boldsymbol{w}_{2,k}, \tag{4}$$

with

$$\boldsymbol{E} = \begin{bmatrix} \boldsymbol{I}_n & \boldsymbol{0} \\ \boldsymbol{0} & \boldsymbol{0} \end{bmatrix}, \quad \boldsymbol{A} = \begin{bmatrix} \bar{\boldsymbol{A}} & \boldsymbol{0} \\ \boldsymbol{0} & \boldsymbol{0} \end{bmatrix}, \quad \boldsymbol{C} = \begin{bmatrix} \bar{\boldsymbol{C}} & \boldsymbol{C}_f \end{bmatrix}, \tag{5}$$

$$\boldsymbol{B} = \begin{bmatrix} \bar{\boldsymbol{B}} \\ \boldsymbol{0} \end{bmatrix}, \quad \boldsymbol{W}_1 = \begin{bmatrix} \bar{\boldsymbol{W}}_1 \\ \boldsymbol{0} \end{bmatrix}, \quad \boldsymbol{W}_2 = \bar{\boldsymbol{W}}_2, \tag{6}$$

and $\boldsymbol{x}_k = [\bar{\boldsymbol{x}}_k^T, \boldsymbol{f}_k^T]^T$. One can easily observe that (3) and (4) constitute a descriptor system with the extended state containing both the original state and the sensor fault. The objective of the subsequent part of this section is to bring (3) and (4) to the classical state-space form with the state shaped by $\boldsymbol{x}_k$. For that purpose, let us start with showing that there exist $\boldsymbol{N}$ and $\boldsymbol{T}$ such that

$$\boldsymbol{T}\boldsymbol{E} + \boldsymbol{N}\boldsymbol{C} = \boldsymbol{I}_{n+s}. \tag{7}$$

Then, we proceed partitioning $\boldsymbol{T}$ as follows:

$$\boldsymbol{T} = \begin{bmatrix} \boldsymbol{T}_1 & \boldsymbol{T}_2 \\ \boldsymbol{T}_3 & \boldsymbol{T}_4 \end{bmatrix}, \tag{8}$$

and hence

$$\boldsymbol{T}\boldsymbol{E} = \begin{bmatrix} \boldsymbol{T}_1 & \boldsymbol{0} \\ \boldsymbol{T}_3 & \boldsymbol{0} \end{bmatrix}. \tag{9}$$

Similarly, let $\boldsymbol{N} = [\boldsymbol{N}_1^T,\ \boldsymbol{N}_2^T]^T$, and hence

$$\boldsymbol{N}\boldsymbol{C} = \begin{bmatrix} \boldsymbol{N}_1\bar{\boldsymbol{C}} & \boldsymbol{N}_1\boldsymbol{C}_f \\ \boldsymbol{N}_2\bar{\boldsymbol{C}} & \boldsymbol{N}_2\boldsymbol{C}_f \end{bmatrix}. \tag{10}$$

Thus, by substituting (9) and (10) into (7), we can show that it is equivalent to

$$\begin{bmatrix} \boldsymbol{T}_1 + \boldsymbol{N}_1\bar{\boldsymbol{C}} & \boldsymbol{N}_1\boldsymbol{C}_f \\ \boldsymbol{T}_3 + \boldsymbol{N}_2\bar{\boldsymbol{C}} & \boldsymbol{N}_2\boldsymbol{C}_f \end{bmatrix} = \boldsymbol{I}_{n+s}. \tag{11}$$

Finally, a solution satisfying the above equality is

$$\boldsymbol{N}_1 = \boldsymbol{0}, \quad \boldsymbol{N}_2 = \boldsymbol{C}_x, \quad \boldsymbol{T}_1 = \boldsymbol{I}_n, \quad \boldsymbol{T}_3 = -\boldsymbol{C}_x\bar{\boldsymbol{C}}, \tag{12}$$

where $\boldsymbol{C}_x$ stands for a general solution to $\boldsymbol{C}_x\boldsymbol{C}_f = \boldsymbol{I}_s$, which is given by

$$\boldsymbol{C}_x = \boldsymbol{C}_f^+ + \boldsymbol{C}_0\left(\boldsymbol{I} - \boldsymbol{C}_f\boldsymbol{C}_f^+\right), \tag{13}$$

where $\boldsymbol{C}_0 \in \mathbb{R}^{s\times m}$ is any arbitrary matrix while $\boldsymbol{C}_f^+$ stands for the pseudoinverse of $\boldsymbol{C}_f$. Moreover, $\boldsymbol{T}_2$ and $\boldsymbol{T}_4$ are arbitrary matrices of appropriate dimensions. This

means that there are infinitely many solutions. However, $\boldsymbol{T}_2$ and $\boldsymbol{T}_4$ have no practical impact, and hence they can be set as $\boldsymbol{T}_2 = \boldsymbol{0}$ and $\boldsymbol{T}_4 = \boldsymbol{0}$. This leads to the final form of matrices $\boldsymbol{T}$ and $\boldsymbol{N}$:

$$\boldsymbol{T} = \begin{bmatrix} \boldsymbol{I}_n & \boldsymbol{0} \\ -\boldsymbol{C}_x\bar{\boldsymbol{C}} & \boldsymbol{0} \end{bmatrix}, \quad \boldsymbol{N} = \begin{bmatrix} \boldsymbol{0} \\ \boldsymbol{C}_x \end{bmatrix}. \tag{14}$$

Thus, by multiplying (3) by $\boldsymbol{T}$ and then substituting $\boldsymbol{TE} = \boldsymbol{I} - \boldsymbol{NC}$, one can get

$$\begin{aligned} \boldsymbol{x}_{k+1} = &\begin{bmatrix} \bar{\boldsymbol{A}} & \boldsymbol{0} \\ -\boldsymbol{C}_x\bar{\boldsymbol{C}}\bar{\boldsymbol{A}} & \boldsymbol{0} \end{bmatrix} \boldsymbol{x}_k + \begin{bmatrix} \boldsymbol{0} & \boldsymbol{0} \\ \boldsymbol{C}_x\bar{\boldsymbol{C}} & \boldsymbol{I}_s \end{bmatrix} \boldsymbol{x}_{k+1} \\ &+ \begin{bmatrix} \bar{\boldsymbol{B}} \\ -\boldsymbol{C}_x\bar{\boldsymbol{C}}\bar{\boldsymbol{B}} \end{bmatrix} \boldsymbol{u}_k + \begin{bmatrix} \bar{\boldsymbol{W}}_1 \\ -\boldsymbol{C}_x\bar{\boldsymbol{C}}\bar{\boldsymbol{W}}_1 \end{bmatrix} \boldsymbol{w}_{1,k}. \end{aligned} \tag{15}$$

Subsequently, using the new state variable, one can multiply the output equation (2) by $\boldsymbol{N}$, which yields

$$\begin{aligned} \begin{bmatrix} \boldsymbol{0} \\ \boldsymbol{C}_x \end{bmatrix} \boldsymbol{y}_{k+1} = &\begin{bmatrix} \boldsymbol{0} & \boldsymbol{0} \\ \boldsymbol{C}_x\bar{\boldsymbol{C}} & \boldsymbol{I}_s \end{bmatrix} \boldsymbol{x}_{k+1} \\ &+ \begin{bmatrix} \boldsymbol{0} \\ \boldsymbol{C}_x\bar{\boldsymbol{W}}_2 \end{bmatrix} \boldsymbol{w}_{2,k+1}. \end{aligned} \tag{16}$$

Finally, substituting (16) into (15) gives a new state-space equation:

$$\begin{aligned} \boldsymbol{x}_{k+1} = &\tilde{\boldsymbol{A}}\boldsymbol{x}_k + \begin{bmatrix} \bar{\boldsymbol{B}} \\ -\boldsymbol{C}_x\bar{\boldsymbol{C}}\bar{\boldsymbol{B}} \end{bmatrix} \boldsymbol{u}_k \\ &+ \begin{bmatrix} \boldsymbol{0} \\ \boldsymbol{C}_x \end{bmatrix} \boldsymbol{y}_{k+1} + \begin{bmatrix} \bar{\boldsymbol{W}}_1 \\ -\boldsymbol{C}_x\bar{\boldsymbol{C}}\bar{\boldsymbol{W}}_1 \end{bmatrix} \boldsymbol{w}_{1,k} \\ &+ \begin{bmatrix} \boldsymbol{0} \\ -\boldsymbol{C}_x\bar{\boldsymbol{W}}_2 \end{bmatrix} \boldsymbol{w}_{2,k+1}, \end{aligned} \tag{17}$$

where

$$\tilde{\boldsymbol{A}} = \begin{bmatrix} \bar{\boldsymbol{A}} & \boldsymbol{0} \\ -\boldsymbol{C}_x\bar{\boldsymbol{C}}\bar{\boldsymbol{A}} & \boldsymbol{0} \end{bmatrix},$$

while the output equation is

$$\begin{aligned} \boldsymbol{y}_k &= [\bar{\boldsymbol{C}}\ \boldsymbol{C}_f]\boldsymbol{x}_k + \bar{\boldsymbol{W}}_2\boldsymbol{w}_{2,k} \\ &= \boldsymbol{C}\boldsymbol{x}_k + \bar{\boldsymbol{W}}_2\boldsymbol{w}_{2,k}. \end{aligned} \tag{18}$$

Note that the form (17) is obtained by a chain of mathematical manipulations, which are inherited from the classical approaches presented, e.g., by Hou and Patton (1998), Hsieh (2011), Chen and Patton (1999) and Witczak (2014). Note that this form involves $\boldsymbol{y}_{k+1}$, and hence, it is not suitable for control purposes. This clearly means that the estimation of the state $\boldsymbol{x}_{k+1}$ requires the measurement $\boldsymbol{y}_{k+1}$. This is also a common strategy in Kalman filter-based approaches (Gillijns and De Moor, 2007). Moreover, as proposed by Hsieh (2011), the state estimation problem can be formed using the descriptor form similar to (3).

3. Development of a fault diagnosis scheme

Having a system description (17)–(18), it is possible to propose a fault diagnosis scheme capable of estimating the faults and states:

$$\begin{aligned} \hat{\boldsymbol{x}}_{k+1} = &\tilde{\boldsymbol{A}}\hat{\boldsymbol{x}}_k + \begin{bmatrix} \bar{\boldsymbol{B}} \\ -\boldsymbol{C}_x\bar{\boldsymbol{C}}\bar{\boldsymbol{B}} \end{bmatrix} \boldsymbol{u}_k \\ &+ \begin{bmatrix} \boldsymbol{0} \\ \boldsymbol{C}_x \end{bmatrix} \boldsymbol{y}_{k+1} + \boldsymbol{K}(\boldsymbol{y}_k - \boldsymbol{C}\hat{\boldsymbol{x}}_k), \end{aligned} \tag{19}$$

where $\boldsymbol{K}$ is an unknown matrix, which has to be determined in such a way as to guarantee the convergence of the estimation error $\boldsymbol{e}_k = \boldsymbol{x}_k - \hat{\boldsymbol{x}}_k$:

$$\boldsymbol{e}_{k+1} = \boldsymbol{X}\boldsymbol{e}_k + \boldsymbol{Y}\tilde{\boldsymbol{w}}_k, \tag{20}$$

where

$$\begin{aligned} &\boldsymbol{X} = \tilde{\boldsymbol{A}} - \boldsymbol{KC}, \\ &\boldsymbol{Y} = \begin{bmatrix} \bar{\boldsymbol{W}}_1 & -\boldsymbol{K}\bar{\boldsymbol{W}}_2 & \boldsymbol{0} \\ -\boldsymbol{C}_x\bar{\boldsymbol{C}}\bar{\boldsymbol{W}}_1 & & -\boldsymbol{C}_x\bar{\boldsymbol{W}}_2 \end{bmatrix}, \end{aligned} \tag{21}$$

while $\tilde{\boldsymbol{w}}_k = [\boldsymbol{w}_{1,k}^T, \boldsymbol{w}_{2,k}^T, \boldsymbol{w}_{2,k+1}^T]^T$.

As mentioned in Section 1, the proposed solution focuses on a single sensor fault. This means that a coverage of all sensor faults is possible by using a bank of (19) (see Fig. 1). This simply implies that each estimator (in the bank of s of them) estimates all faults but it is designed in such a way as to provide an estimate of the i-th ($i = 1, \ldots, s$) fault with as little uncertainty as possible.

The objective of the subsequent part of this section is to perform a comprehensive convergence analysis of the estimation error (20). For that purpose, let us start with defining a Lyapunov function $V_k = \boldsymbol{e}_k^T\boldsymbol{P}\boldsymbol{e}_k$, $\boldsymbol{P} \succ 0$. In the deterministic case, $\tilde{\boldsymbol{w}}_k = \boldsymbol{0}$ in (20), and hence the conventional Lyapunov approach can be employed. On the other hand, for $\tilde{\boldsymbol{w}}_k \neq \boldsymbol{0}$, suitable assumptions about $\tilde{\boldsymbol{w}}_k$ should be performed. To settle this problem, the celebrated $\mathcal{H}_\infty$ approach along with an alternative strategy called quadratic boundedness (QB) (Alessandri *et al.*, 2006; Ding, 2010; Pazera and Witczak, 2019) can be employed. Thus, for the purpose of further discussion, the following definitions are introduced:

Definition 1. The estimator (19) is convergent in the $\mathcal{H}_\infty$ sense iff (20) satisfies

$$V_{k+1} - V_k + \boldsymbol{e}_k^T\boldsymbol{e}_k - \mu^2\tilde{\boldsymbol{w}}_k^T\tilde{\boldsymbol{w}}_k < 0, \tag{22}$$

where $\mu > 0$ is a disturbance attenuation level and $\tilde{\boldsymbol{w}}_k \in l_2$ whilst (Zemouche *et al.*, 2008)

$$\begin{aligned} l_2 &= \{\tilde{\boldsymbol{w}} \in \mathbb{R}^{n_w} \,|\, \|\tilde{\boldsymbol{w}}\|_{l_2} < +\infty\}, \\ \|\tilde{\boldsymbol{w}}\|_{l_2} &= \Big(\sum_{k=0}^{\infty} \|\tilde{\boldsymbol{w}}_k\|^2\Big)^{\frac{1}{2}}. \end{aligned} \tag{23}$$

Definition 2. The estimator (19) is convergent in the QB sense iff (20) satisfies

$$V_{k+1} - (1-\alpha)\, V_k - \alpha \tilde{\boldsymbol{w}}_k^T \boldsymbol{Q}_w \tilde{\boldsymbol{w}}_k < 0, \qquad (24)$$

where $0 < \alpha < 1$ for all $\tilde{\boldsymbol{w}}_k \in \mathcal{E}$ satisfying

$$\mathcal{E} = \left\{ \tilde{\boldsymbol{w}} : \tilde{\boldsymbol{w}}^T \boldsymbol{Q}_w \tilde{\boldsymbol{w}} \leq 1 \right\}, \quad \boldsymbol{Q}_w \succ 0. \qquad (25)$$

Comparing (22) and (24), we can observe a similarity between them. This feature enables formulating the following unifying framework:

$$V_{k+1} - V_k + \boldsymbol{e}_k^T \boldsymbol{R} \boldsymbol{e}_k - \tilde{\boldsymbol{w}}_k^T \boldsymbol{Q} \tilde{\boldsymbol{w}}_k < 0, \qquad (26)$$

with $\boldsymbol{R} \succeq 0$ as well as $\boldsymbol{Q} \succeq 0$.

Thus, by substituting the following values to (26), we can obtain

- Lyapunov approach: $\boldsymbol{R} = \boldsymbol{0}, \boldsymbol{Q} = \boldsymbol{0}$,
- QB approach: $\boldsymbol{R} = \alpha \boldsymbol{P}, \boldsymbol{Q} = \alpha \boldsymbol{Q}_w$,
- $\mathcal{H}_\infty$ approach: $\boldsymbol{R} = \boldsymbol{I}, \boldsymbol{Q} = \mu^2 \boldsymbol{I}$.

Before proceeding to the main result of this section, let us recall Finsler's lemma (Skelton *et al*., 1997).

Lemma 1. *The following properties are equivalent:*

1. $\tilde{\boldsymbol{e}}^T \boldsymbol{E} \tilde{\boldsymbol{e}} < 0, \quad \forall \tilde{\boldsymbol{e}} \in \{\tilde{\boldsymbol{e}} \in \mathbb{R}^{n+s} | \tilde{\boldsymbol{e}} \neq 0, \boldsymbol{F}\tilde{\boldsymbol{e}} = 0\}$,
2. $\exists \boldsymbol{M} \in \mathbb{R}^{n+s \times m}$ *such that* $\boldsymbol{E} + \boldsymbol{M}\boldsymbol{F} + \boldsymbol{F}^T \boldsymbol{M}^T \prec 0$.

Theorem 1. *The system* (20) *satisfies* (26) *iff there exist matrices* $\boldsymbol{P} \succ \boldsymbol{0}$, $\boldsymbol{R} \succeq \boldsymbol{0}$, $\boldsymbol{Q} \succeq \boldsymbol{0}$ $\boldsymbol{U}$, $\boldsymbol{L}$ *for which*

$$\begin{bmatrix} -\boldsymbol{P} + \boldsymbol{R} & \boldsymbol{0} & \tilde{\boldsymbol{A}}^T \boldsymbol{U}^T - \boldsymbol{C}^T \boldsymbol{L}^T \\ \boldsymbol{0} & -\boldsymbol{Q} & \boldsymbol{D}^T \\ \boldsymbol{U}\tilde{\boldsymbol{A}} - \boldsymbol{L}\boldsymbol{C} & \boldsymbol{D} & \boldsymbol{P} - \boldsymbol{U} - \boldsymbol{U}^T \end{bmatrix} \prec 0, \qquad (27)$$

$$\boldsymbol{D} = \left[\boldsymbol{U} \begin{bmatrix} \bar{\boldsymbol{W}}_1 \\ -\boldsymbol{C}_x \bar{\boldsymbol{C}} \bar{\boldsymbol{W}}_1 \end{bmatrix} - \boldsymbol{L} \bar{\boldsymbol{W}}_2 \; \boldsymbol{U} \begin{bmatrix} \boldsymbol{0} \\ -\boldsymbol{C}_x \bar{\boldsymbol{W}}_2 \end{bmatrix} \right]. \qquad (28)$$

Proof. Definine the following super-vector:

$$\tilde{\boldsymbol{e}}_k = \left[\boldsymbol{e}_k^T, \tilde{\boldsymbol{w}}_k^T, \boldsymbol{e}_{k+1}^T \right]^T. \qquad (29)$$

As a result, (20) can be rewritten in the form

$$[\boldsymbol{X} \; \boldsymbol{Y} \; -\boldsymbol{I}] \, \tilde{\boldsymbol{e}}_k = \boldsymbol{F} \tilde{\boldsymbol{e}}_k = \boldsymbol{0}. \qquad (30)$$

Moreover, define

$$\boldsymbol{Z} = \operatorname{diag}(-\boldsymbol{P} + \boldsymbol{R}, -\boldsymbol{Q}, \boldsymbol{P}), \quad \boldsymbol{M} = \begin{bmatrix} \boldsymbol{0} \\ \boldsymbol{0} \\ \boldsymbol{U} \end{bmatrix}. \qquad (31)$$

Finally, using Finsler's lemma yields

$$\begin{bmatrix} -\boldsymbol{P} + \boldsymbol{R} & \boldsymbol{0} & \boldsymbol{X}^T \boldsymbol{U}^T \\ \boldsymbol{0} & -\boldsymbol{Q} & \boldsymbol{Y}^T \boldsymbol{U}^T \\ \boldsymbol{U}\boldsymbol{X} & \boldsymbol{U}\boldsymbol{Y} & \boldsymbol{P} - \boldsymbol{U} - \boldsymbol{U}^T \end{bmatrix} \prec \boldsymbol{0}. \qquad (32)$$

Inserting

$$\begin{aligned} \boldsymbol{U}\boldsymbol{X} &= \boldsymbol{U}\left(\tilde{\boldsymbol{A}} - \boldsymbol{K}\boldsymbol{C}\right) = \boldsymbol{U}\tilde{\boldsymbol{A}} - \boldsymbol{L}\boldsymbol{C}, \qquad (33) \\ \boldsymbol{U}\boldsymbol{Y} &= \boldsymbol{D} \end{aligned}$$

into (32) completes the proof. ∎

The practical application of Theorem 1 boils down to selecting either

- the $\mathcal{H}_\infty$ approach by setting $\boldsymbol{R} = \boldsymbol{I}$, $\boldsymbol{Q} = \mu^2 \boldsymbol{I}$ in (27), or
- the QB approach by setting $\boldsymbol{R} = \alpha \boldsymbol{P}$, $\boldsymbol{Q} = \alpha \boldsymbol{Q}_w$ in (27),

and then solving (27). In both the cases, a bilinear matrix inequality is obtained with respect to either μ or α, respectively. Such a problem can be solved by choosing either μ or α from a predefined set and then solving (27). Alternatively, the problem can transformed into a generalized eigenvalue one (Witczak, 2007).

Irrespective of the selected approach, the estimator (19) gain matrix can be calculated as follows:

$$\boldsymbol{K} = \boldsymbol{U}^{-1} \boldsymbol{L}. \qquad (34)$$

Note that the regularity of $\boldsymbol{U}$ is ensured by the fact that satisfying (27) implies $\boldsymbol{P} - \boldsymbol{U}^T - \boldsymbol{U} \prec 0$. Finally, it should be noted that the selection of matrix $\boldsymbol{M}$ in (31) is not accidental. Indeed, as proven by de Oliveira *et al*. (1999), such an approach is equivalent to the usual Lyapunov matrix inequality-based strategy. However, as indicated by de Oliveira and Skelton (2007), replacing zero entries of $\boldsymbol{M}$ in (31) may provide some additional design freedom, which can be beneficial while obtaining the numerical solutions of (27).

Having (17) and (18), the observability condition of the pair $(\tilde{\boldsymbol{A}}, \boldsymbol{C})$ should be checked, which boils down to verifying the rank of the observability matrix

$$\operatorname{rank}(\mathcal{O}) = n + s, \quad \mathcal{O} = \begin{bmatrix} \boldsymbol{C} \\ \boldsymbol{C}\tilde{\boldsymbol{A}} \\ \boldsymbol{C}\tilde{\boldsymbol{A}}^2 \\ \vdots \\ \boldsymbol{C}\tilde{\boldsymbol{A}}^{n+s-1} \end{bmatrix}. \qquad (35)$$

Let us start with noting that

$$\begin{aligned} \tilde{\boldsymbol{A}}^b &= \begin{bmatrix} \bar{\boldsymbol{A}}^b & \boldsymbol{0} \\ -\boldsymbol{C}_x \bar{\boldsymbol{C}} \bar{\boldsymbol{A}}^b & \boldsymbol{0} \end{bmatrix}, \\ \boldsymbol{C}\tilde{\boldsymbol{A}}^b &= \left[[\boldsymbol{I}_m - \boldsymbol{C}_f \boldsymbol{C}_x] \bar{\boldsymbol{C}} \bar{\boldsymbol{A}}^b \quad \boldsymbol{0} \right]. \end{aligned} \qquad (36)$$

Thus, the observability condition becomes

$$\text{rank}(\mathcal{O}) = n + s,$$
$$\mathcal{O} = \begin{bmatrix} \bar{\boldsymbol{C}} & \boldsymbol{C}_f \\ [\boldsymbol{I}_m - \boldsymbol{C}_f\boldsymbol{C}_x]\bar{\boldsymbol{C}}\bar{\boldsymbol{A}} & \boldsymbol{0} \\ [\boldsymbol{I}_m - \boldsymbol{C}_f\boldsymbol{C}_x]\bar{\boldsymbol{C}}\bar{\boldsymbol{A}}^2 & \boldsymbol{0} \\ \vdots & \vdots \\ [\boldsymbol{I}_m - \boldsymbol{C}_f\boldsymbol{C}_x]\bar{\boldsymbol{C}}\bar{\boldsymbol{A}}^{n+s-1} & \boldsymbol{0} \end{bmatrix}. \tag{37}$$

Since $\boldsymbol{I}_m - \boldsymbol{C}_f\boldsymbol{C}_x$ is an idempotent matrix, it is evident that

$$\begin{aligned} \text{rank}(\boldsymbol{I}_m - \boldsymbol{C}_f\boldsymbol{C}_x) &= m - \text{rank}(\boldsymbol{C}_f\boldsymbol{C}_x) \\ &= m - \text{rank}(\boldsymbol{C}_f) = m - s, \end{aligned} \tag{38}$$

which clearly proves that the number of sensors should be larger than that of faults being considered, $m > s$. Note also that the choice of $\boldsymbol{C}_0$ has no impact on observability, and hence it does not influence the final estimator design problem.

As a result of the above-performed analysis, the following conclusions can be drawn:

- A necessary condition for the observability of the pair $(\tilde{\boldsymbol{A}}, \boldsymbol{C})$ is that $m > s$.
- Together, $m > s$ and $\text{rank}(\mathcal{O}) = n + s$ form a necessary and sufficient condition for the observability of $(\tilde{\boldsymbol{A}}, \boldsymbol{C})$.
- The observability of $(\tilde{\boldsymbol{A}}, \boldsymbol{C})$ is a necessary condition for the existence of a solution of (27).

Obviously, the proposed fault estimation scheme refers to sensor faults and this is undoubtedly important. However, the descriptor-based scheme can be easily transformed to actuator fault estimation, or both sensor and actuator fault estimation, which might appear simultaneously. Such schemes can be found, e.g., in the work of Witczak *et al*. (2022), Kukurowski *et al.* (2021a; 2021b), Pazera and Witczak (2019) or Pazera *et al*. (2021).

4. Determining a minimum detectable fault

Irrespective of the fault and state estimation scheme being used, it always provides estimates with an associated uncertainty. Thus, instead of a point estimate, a fault uncertainty interval is obtained. It can be formally defined as

$$f_{i,k} \in \mathbb{F}_i, \quad \mathbb{F}_i = \left[\underline{f}_{i,k}, \overline{f}_{i,k}\right], \quad i = 1, \ldots, s, \tag{39}$$

where $\underline{f}_{i,k} \leq \overline{f}_{i,k}$ stand for its lower and upper bound, respectively. This means that any value contained in $\mathbb{F}_i$ is an equally good estimate of $f_{i,k}$. As a consequence,

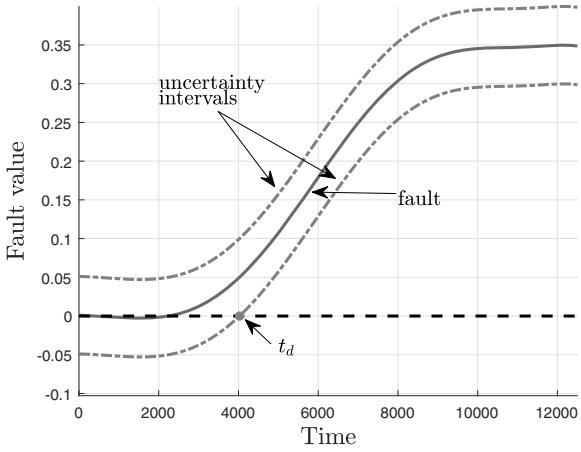

Fig. 2. Fault uncertainty interval and the fault detection time t_d.

the fault detection time t_d is defined as a time instance at which one of the extremities of $\mathbb{F}_i$ gets zero. Such a situation is illustrated in Fig. 2. The most common approach to form the fault uncertainty interval is to use the fault estimate along with the knowledge of its uncertainty expressed by o_i, i.e.,

$$\mathbb{F}_i = \left[\underline{f}_{i,k}, \overline{f}_{i,k}\right] = \left[\hat{f}_{i,k} - o_{i,k}, \hat{f}_{i,k} + o_{i,k}\right], \tag{40}$$

$i = 1, \ldots, s$. Thus, the fault is detected if either $\hat{f}_{i,k} - o_{i,k} \geq 0$ or $\hat{f}_{i,k} + o_{i,k} \leq 0$ are satisfied. This clearly means that the minimum detectable fault is the one for which $\hat{f}_{i,k} \geq o_{i,k}$ or $\hat{f}_{i,k} \leq -o_{i,k}$. As a result, the MDF depends solely on $o_{i,k}$.

The objective of the subsequent part of this section is to provide a way for determining the form as well as the minimum value of $o_{i,k}$. Let us start with recalling that (26) can be written as

$$V_{k+1} < \boldsymbol{e}_k^T(\boldsymbol{P} - \boldsymbol{R})\boldsymbol{e}_k + \tilde{\boldsymbol{w}}_k^T\boldsymbol{Q}\tilde{\boldsymbol{w}}_k. \tag{41}$$

Moreover, the satisfaction of (27) implies $\boldsymbol{P} - \boldsymbol{R} \succ \boldsymbol{0}$. This means that there exists a scalar $\gamma \in (0, 1)$ such that

$$\boldsymbol{e}_k^T\boldsymbol{R}\boldsymbol{e}_k \leq \gamma\boldsymbol{e}_k^T\boldsymbol{P}\boldsymbol{e}_k, \tag{42}$$

Note that, in the QB case, $\boldsymbol{R} = \alpha\boldsymbol{P}$, and hence the above nonstrict inequality becomes an equality with $\gamma = \alpha$. Thus, substituting (42) and $\boldsymbol{Q} = \gamma\boldsymbol{Q}_\gamma$ ($\boldsymbol{Q}_\gamma \succ \boldsymbol{0}$) yields

$$V_{k+1} - (1 - \gamma)V_k < \gamma\tilde{\boldsymbol{w}}_k^T\boldsymbol{Q}_\gamma\tilde{\boldsymbol{w}}_k. \tag{43}$$

Again, note that, in the QB case, $\boldsymbol{Q}_\gamma = \boldsymbol{Q}_w$ and $\tilde{\boldsymbol{w}}_k^T\boldsymbol{Q}_\gamma\tilde{\boldsymbol{w}}_k \leq 1$. Thus, to guarantee the boundedness of (43) in the $\mathcal{H}_\infty$ case, a similar assumption has to be imposed, i.e., $\tilde{\boldsymbol{w}}_k^T\boldsymbol{Q}_\gamma\tilde{\boldsymbol{w}}_k \leq 1$. Under such an assumption, the inequality (43) can be simply written as

$$V_{k+1} - (1 - \gamma)V_k < \gamma. \tag{44}$$

Subsequently, by applying induction to (44), we can get

$$V_k \leq (1-\gamma)^k V_0 + \gamma \sum_{i=0}^{k-1} (1-\gamma)^i, \tag{45}$$

and finally,

$$V_k \leq \psi(\gamma) = (1-\gamma)^k (V_0 - 1) + 1. \tag{46}$$

Irrespective of V_0, the relation (46) converges to $V_k \leq 1$, i.e., $\boldsymbol{e}_k \boldsymbol{P} \boldsymbol{e}_k \leq 1$. This means that the fault uncertainty interval is given by

$$\begin{aligned} &f_{j,k} \in \mathbb{F}_j, \\ &\mathbb{F}_j = \left[\hat{f}_{j,k} - \sqrt{\psi(\gamma) \boldsymbol{c}_i^T \boldsymbol{P}^{-1} \boldsymbol{c}_i}, \right. \\ &\qquad \left. \hat{f}_{j,k} + \sqrt{\psi(\gamma) \boldsymbol{c}_i^T \boldsymbol{P}^{-1} \boldsymbol{c}_i} \right], \end{aligned} \tag{47}$$

where $\boldsymbol{c}_i$ is a column of the $n+s$ identity matrix while $i = n + j$ and $j = 1, \ldots, s$.

As already mentioned, the size of the minimum detectable fault is proportional to $o_{j,k} = \sqrt{\psi(\gamma) \boldsymbol{c}_i^T \boldsymbol{P}^{-1} \boldsymbol{c}_i}$. Thus, to derive its optimal value, the following minimization problem is formulated:

$$\min_{\boldsymbol{P} \succ \boldsymbol{0}} \boldsymbol{c}_i^T \boldsymbol{P}^{-1} \boldsymbol{c}_i \tag{48}$$

subject to (27). To make the above problem tractable, i.e., to eliminate the inverse of $\boldsymbol{P}$, it is assumed that there exists a scalar $\beta > 0$ satisfying

$$\boldsymbol{c}_i^T \boldsymbol{P}^{-1} \boldsymbol{c}_i \leq \beta, \tag{49}$$

which, by employing the Schur complement, can be transformed into an LMI:

$$\begin{bmatrix} -\beta & \boldsymbol{c}_i^T \\ \boldsymbol{c}_i & -\boldsymbol{P} \end{bmatrix} \leq \boldsymbol{0}. \tag{50}$$

Finally, it should be noted that minimizing (48) under (27) is equivalent to

$$\min_{\beta > 0} \beta \tag{51}$$

under (27) and (50). This leads directly to the following iterative design procedure:

Step 0: Choose a maximum allowable bound of β, i.e., $\bar{\beta}$, and its iteration step $\Delta_\beta > 0$. Choose the minimum convergence factor $\underline{\gamma} \in (0, 1)$ along with the iteration step $\Delta_\gamma > 0$. Set $\beta = \bar{\beta}$.

Step 1: Set $\gamma = \underline{\gamma}$.

Step 2: If possible, obtain a feasible solution of (27) and (50).

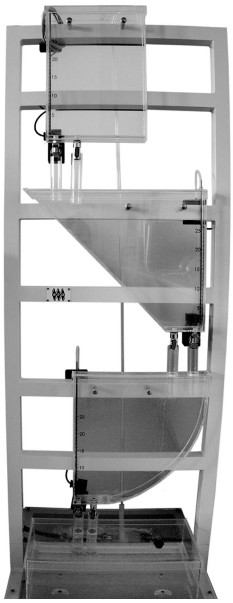

Fig. 3. Multi-tank system.

Step 3: If $\gamma + \Delta_\gamma < 1$, set $\gamma = \gamma + \Delta_\gamma$; otherwise, go to Step 4.

Step 4: If $\beta - \Delta_\beta > 0$, then update $\beta = \beta - \Delta_\beta$ and proceed to Step 1.

As a result of applying the above procedure, a grid of possible (γ, β) solutions is obtained. Finally, the most well-suited one can be selected.

5. Sample results

5.1. Simulation study. The minimum detectable sensor fault approach is verified using the multi-tank (MT) system portrayed in Fig. 3. The examined system is fully computer-based controlled, which facilitates the implementation of various control, identification, and estimation strategies. The system consists of three vertically arranged tanks with different volumes and shapes. A fully controlled water pump supplies liquid to the top tank. The liquid then flows sequentially from the top tank to the middle one and then to the lower one before ultimately reaching the reservoir. To achieve control over the interconnections between the tanks, solenoid valves are employed and adjusted using a pulse width modulation (PWM) signal. Also, the PWM signal is utilized to control the pump's behaviour. The water levels in the tanks are measured through water pressure readings. The system considered offers three different control modes, each serving specific purposes:

1. *Pump Control:* This mode is the most popular and simplest approach. It allows stabilizing the water

level in a single tank by adjusting the pump's control signal while keeping all the valves open permanently.

2. *Valve Control:* In this mode, the water level in all three tanks can be simultaneously stabilized by adjusting the control signals of the valves. However, the pump operates with a constant flow, limiting the achievable water levels.

3. *Pump-Valve Control:* This is the most interesting and challenging mode. It enables the stabilization of the water level in each tank and, unlike in the previous mode, a predefined water level in each tank can be achieved.

In summary, the system offers great flexibility, with the pump-valve control mode providing the most comprehensive control over the water levels in the tanks. However, the primary objective is to test the performance of the sensor fault estimation schemes, and hence a simple pump control is used exclusively.

The nonlinear model of the system (Pazera and Witczak, 2019) is linearized and discretized (INTECO, 2013). This is realized under a sampling time of $T_s = 0.01$ seconds, which leads to the following system matrices:

$$\bar{\boldsymbol{A}} = \begin{bmatrix} 0.9997 & 0 & 0 \\ 0.0004088 & 0.9995 & 0 \\ 7.318e-08 & 0.0003579 & 0.9997 \end{bmatrix},$$

$$\bar{\boldsymbol{B}} = \begin{bmatrix} 1.143 \\ 0 \\ 0 \end{bmatrix}, \qquad \bar{\boldsymbol{C}} = \begin{bmatrix} 1 & 0 & 0 \\ 0 & 1 & 0 \\ 0 & 0 & 1 \end{bmatrix}, \tag{52}$$

$$\bar{\boldsymbol{W}}_1 = 0.05\boldsymbol{I}_n, \qquad \bar{\boldsymbol{W}}_2 = 0.01\boldsymbol{I}_m.$$

The distribution matrices $\bar{\boldsymbol{W}}_1$ and $\bar{\boldsymbol{W}}_2$ should express the influence and magnitude of $\boldsymbol{w}_k$ onto the state and output (1) and (2), respectively. To obtain an appropriate proportion between the elements of $\bar{\boldsymbol{W}}_1$ and $\bar{\boldsymbol{W}}_2$, a series of constant liquid level measurements were performed for the top tank. Subsequently, the mean was subtracted, which represents the constant liquid level, and then the disturbances where analyzed. The standard deviation of the disturbance obtained for a series of measurements is equal to $1.75 \cdot 10^{-4}$. Almost identical results were obtained for the sensors in the middle and bottom tanks. As a result, the above settings of the distribution matrices were established. Moreover, $\boldsymbol{w}_1$ and $\boldsymbol{w}_2$ were generated according to the truncated normal distribution with expectations equal to 0, standard deviations σ_{w_1} and σ_{w_2}, and the truncation level equal to $4 \cdot 10^{-4}$ and $2 \cdot 10^{-4}$, respectively.

The sensor fault distribution matrix $\boldsymbol{C}_f$ is defined with components of ones and zeros, where the value of one indicates that the fault affects the corresponding sensor readings while zero signifies the opposite. In the second sensor case, this matrix is set as follows:

$$\boldsymbol{C}_f = \begin{bmatrix} 0 \\ 1 \\ 0 \end{bmatrix}. \tag{53}$$

All the three liquid levels were measured, but the sensor in the middle tank was impaired by a fault. Such a configuration of the system allows defining a scenario for investigating the fault estimation process which is given as follows:

F-Sc:

$$f_{2,k} = \begin{cases} 0.05 \cdot \sum\limits_{i=1}^{4} p_{c,i} \cdot k^{|i-4|}, & 5001 \leq k \leq 11500, \\ 0.105, & k \geq 11501, \\ 0, & \text{otherwise}, \end{cases} \tag{54}$$

where $f_{2,k}$ stands for a fault signal corresponding to the level sensor in the second (middle) tank at time k, with p_c denoting a coefficient vector,

$$p_c = \left[-2 \cdot 10^{-15}, 3 \cdot 10^{-13}, -9 \cdot 10^{-11}, 5 \cdot 10^{-6} \right]. \tag{55}$$

It should be noted that this is only a function that describes the behaviour of a real fault applied to the system and does not have any direct impact on the estimation error. In other words, the function describes the shape of a real fault. Such a fault scenario allows examining the fault estimation approach in two ways. Firstly, the sensor fault is slowly developing and then it starts to rise in an exponential way. Finally, the readings show a value that is 10 cm higher than it really is in the tank. The proposed iterative estimator design procedure requires $\bar{\beta}$ as an initialization parameter. Indeed, for a real system, its value can be easily assessed. In the proposed strategy, the maximum value of the minimum detectable sensor fault is assumed to be $\bar{\beta} = 0.35$. Such an assumption simply stems from the highest water level which might be reached in each tank.

This assumption enables the calculation of the relationship between two important parameters: the convergence rate $0 < \gamma < 1$ and the minimum detectable fault bound $0 < \beta < \bar{\beta}$. The results obtained from this analysis are depicted in Fig. 4. The dots on the graph represent situations where a numerical solution can be found for a specific combination of γ and β.

It can be observed from (46) that the higher γ, the higher the convergence rate. This simply means that it is harder to design an estimator, which is clearly visible in Fig. 4. In cases where such a combination is not feasible,

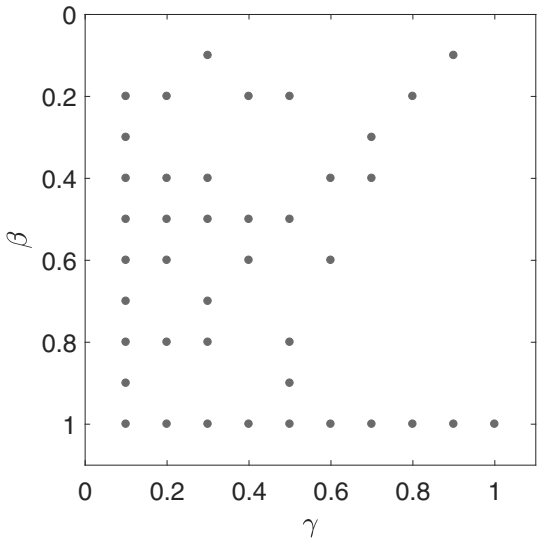

Fig. 4. Convergence rate γ vs. bound β on the uncertainty interval.

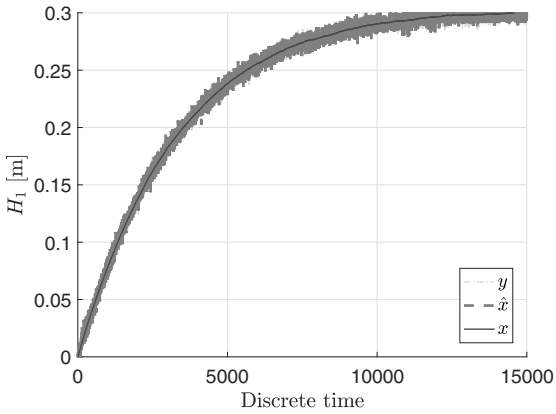

Fig. 5. State values of the first tank—simulation study.

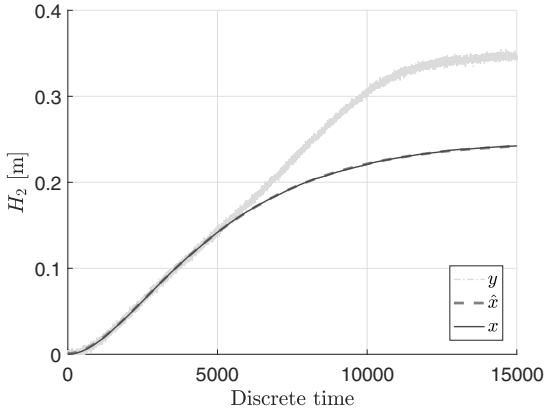

Fig. 6. State values of the second tank—simulation study.

the numerical optimization problem remains unsolvable. Thus, one can clearly observe also some unappealing features of the solver itself.

It is important to note that the dots in the figure indicate that a solution can be obtained for a given configuration of γ and β. Otherwise, a solution cannot be obtained. The experiment was conducted in an open-loop setup, where the control signal for the pump was kept constant throughout the entire duration of the experiment. Specifically, the water pump operated at 50% efficiency during the entire time span, while the solenoid-valves remained fully opened.

Figures 5–7 display the system's response. In these figures, the solid lines represent the states, the dashed lines indicate the estimates, and the dash-dotted lines represent the measured outputs.

As can be observed, the state estimates exhibit a remarkable accuracy, even in the presence of considerable measurement disturbances. In all three cases, the state estimates quickly converge to the actual states. Thus, the state estimation can be considered a highly appropriate one. The sensor fault estimation results are presented in Fig. 8. The dashed line represents the real fault impact on the system and the solid one corresponds to the fault estimate. It is important to note that the real fault is shown for illustration purposes only, and its estimate was obtained solely based on the system model and the estimator's structure, without any prior knowledge of its shape and magnitude.

The fault estimate demonstrates a relatively high level of accuracy, i.e., it follows the true fault while being influenced by some small disturbances. These disturbances cause the estimates to oscillate around a specific value with a relatively small amplitude. Note that the estimator was able to accurately reconstruct the sensor faults, regardless of whether they were abrupt, constant or slowly developing ones. The fault estimate demonstrates a quick and precise response to changes related to the real fault. Figure 9 portrays the thresholds obtained with the proposed approach (cf. Section 4), which are marked as the optimal ones.

The proposed methodology was compared with other methods widely available in the literature (Mustafa *et al.*, 2016), which are marked as the SMI technique. The compared approach is also based on the minimum identified uncertainty bounds violation. However, such a methodology relies on the set membership identification (SMI) technique. Indeed, the proposed approach allowed achieving narrower thresholds. This clearly determines the minimum detectable fault. Moreover, the convergence of the estimator is strictly related to parameters γ and β. Figure 10 shows the evolution of the trace of $\boldsymbol{P}$ while changing these dependent parameters.

As can be observed, a minor change in the trace is observed while changing β and γ. This can be clearly

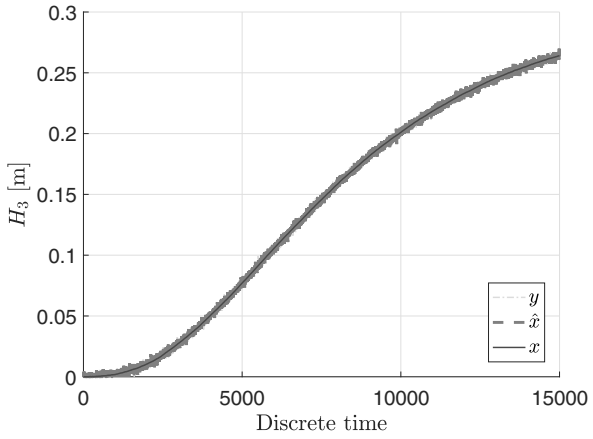

Fig. 7. State values of the third tank—simulation study.

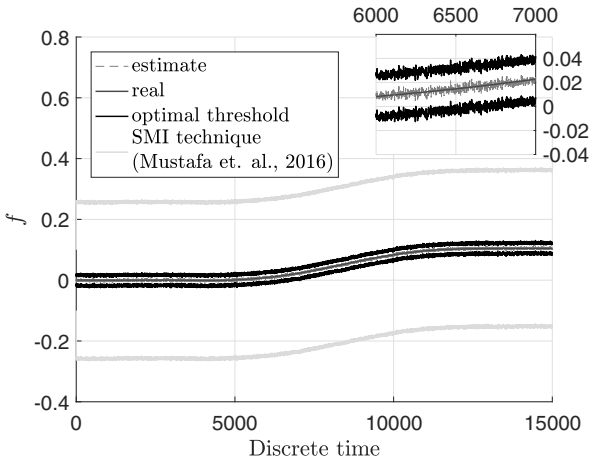

Fig. 9. Comparison of optimal and non-optimal uncertainty intervals for the fault estimate—simulation study.

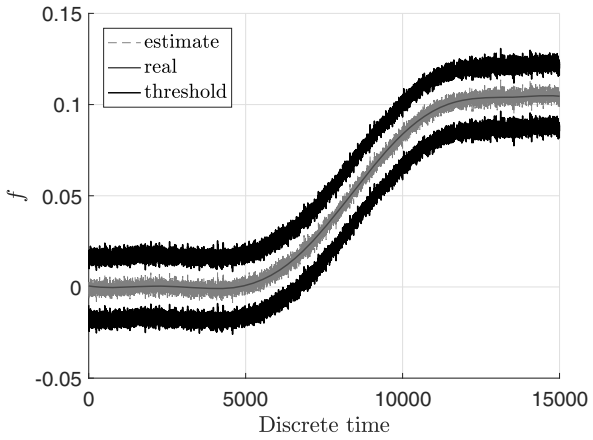

Fig. 8. Sensor fault and its estimate along with uncertainty intervals—simulation study.

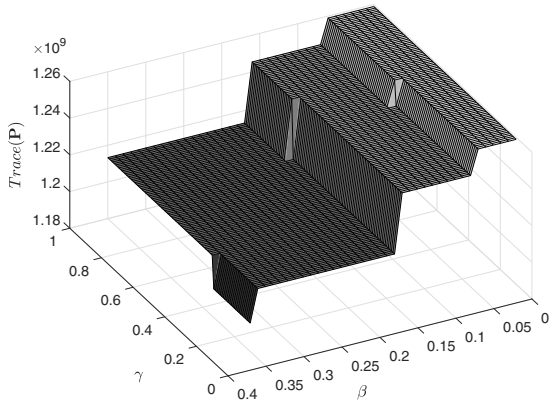

Fig. 10. Evolution of trace $(\boldsymbol{P})$.

explained by the fact that a decrease in one sensor fault uncertainty interval causes an increase in the others. As a result, the trace remains almost untouched.

5.2. Application to a real system. This subsection is concerned with the application to a real MT system. According to the model of the system, it is a nonlinear one (INTECO, 2013; Witczak, 2014). However, to deal with nonlinearities, the proposed approach can be easily extended by handling the nonlinear function describing the behaviour of the system. With such an extension, the estimator can be obtained, e.g., using the linear parameter varying (LPV) technique (Zemouche and Boutayeb, 2013). In such a case, the estimator is calculated not only for the linear model. Rather, the estimator is obtained for all vertices (sub-models) of the LPV model. To compare the experimental study with simulations, the same fault scenario (54) was performed to validate the correctness of the proposed approach. Figures 11–13 show the results obtained with the real system. In these figures, the output of the system is presented with dash-dotted lines while the real state is given by solid ones. Moreover, the state estimate is portrayed with the dashed line.

It should be noted that the estimation process was based only on measurement data and the real state of the system is portrayed in these figures only for informative purposes. The real states were measured additionally while the system was performing and the signals were supplementarily filtered with a simple first order low-pass filter. It can be easily noticed that the states were estimated properly despite the sensor fault occurrence. The magnifying windows docked into these figures show the accuracy and convergence of the proposed approach.

Furthermore, Fig. 14 portrays the sensor fault which was introduced into the real system. The real fault is presented with the solid line while its estimate is given

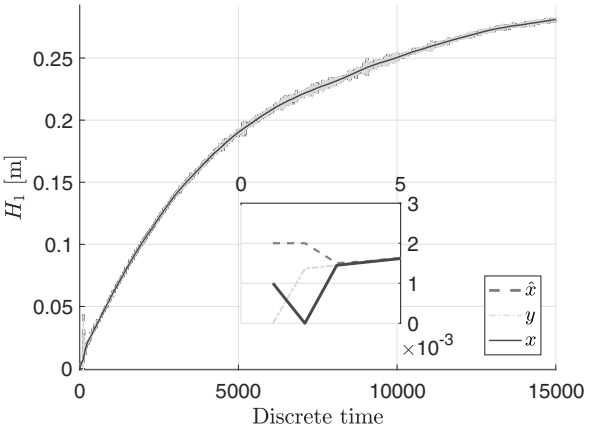

Fig. 11. Water level in the top tank—experimental study.

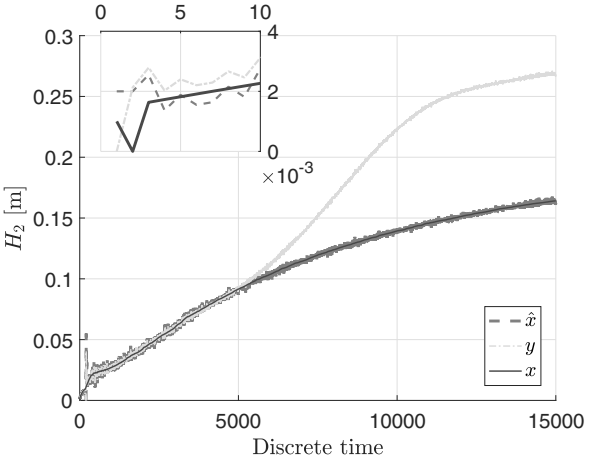

Fig. 12. Water level in the middle tank—experimental study.

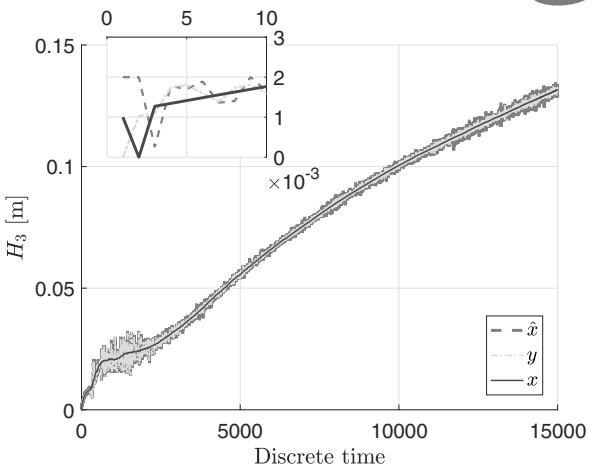

Fig. 13. Water level in the lower tank—experimental study.

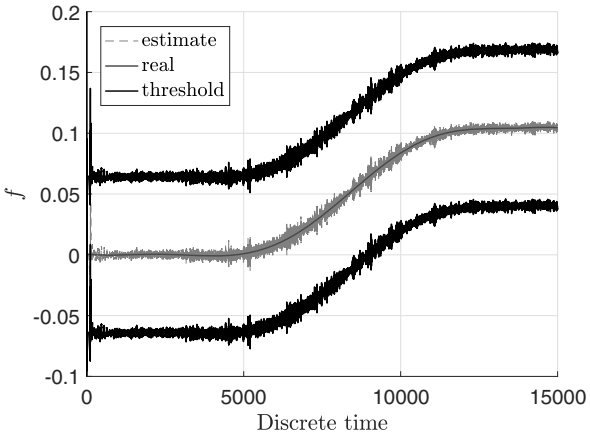

Fig. 14. Sensor fault and its estimate along with uncertainty intervals—experimental study.

by a dashed one. Moreover, the thresholds are presented with the black solid lines. It can be easily seen that the fault is estimated with a good accuracy. The real fault in this figure is presented only for the information purpose. It is not taken into account during the estimation process. The fault estimate is obtained based on the measurements and estimator structure exclusively.

It should be noticed that in both the cases—simulation study as well as the application to the real system—the faults were estimated in a very proper way. Moreover, the uncertainty intervals obtained during the simulation study are slightly narrower. For the clarity of presentation, the comparison results are included in Table 1. It can be easily shown that the mean as well as the standard deviation of the distance of the bound from the real fault are much lower in the proposed approach for simulation and experimental studies than in the SMI technique developed by Mustafa *et al.* (2016).

For better presentation, Fig. 15 shows the state estimation error. It can be clearly seen that it is influenced by disturbances.

For comparison purposes, a case with two available sensors was considered as well. For that purpose, the following setting was employed:

$$\boldsymbol{C} = \begin{bmatrix} 1 & 0 & 0 \\ 0 & 1 & 0 \end{bmatrix}, \tag{56}$$

which corresponds to the fact that the sensor in the bottom tank is not available. Due the lack of space, only the immeasurable state along with the sensor fault is portrayed in Figs. 16 and 17. As can be noticed, despite the fact that the bottom tank water level was immeasurable, the state as well as the fault were estimated properly.

6. Conclusions

The main objective of this paper was to propose an estimation strategy for sensor faults, which guarantees as little uncertainty as possible. Subsequently, the

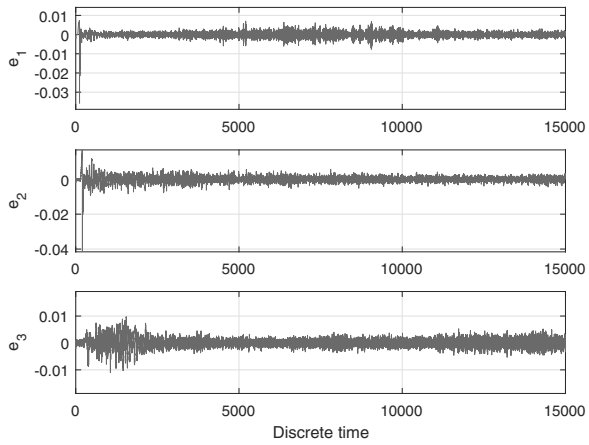

Fig. 15. State estimation error.

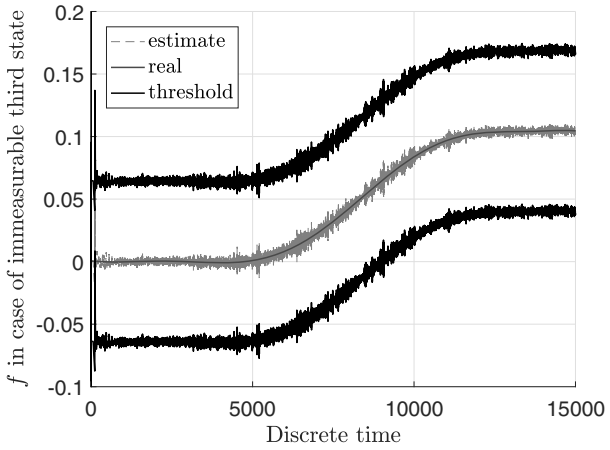

Fig. 16. Sensor fault and its estimate in the case of an unmeasurable state of the bottom tank—experimental study.

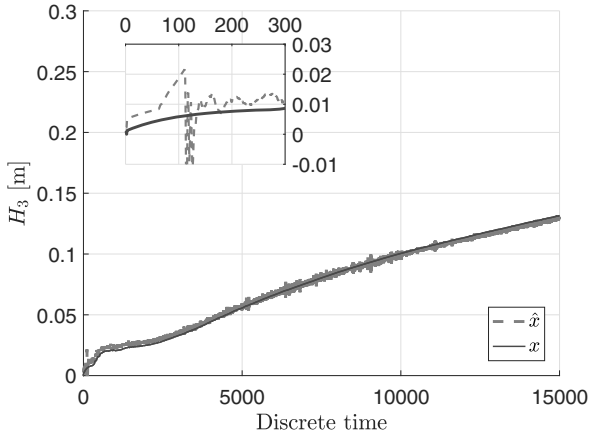

Fig. 17. Water level in the lower tank in the case of an unmeasurable state—experimental study.

Table 1. Comparison table.

	Mean	Standard deviation
Simulation study	0.017	0.0023
Experimental study	0.0642	0.0038
SMI technique	0.2571	0.0027

level of such an uncertainty is utilized to define the so-called minimum detectable sensor fault. Additionally, a guaranteed exponential convergence rate is achieved as well. In particular, the developments started with converting a given class of linear dynamic systems into equivalent descriptor ones. Subsequently, a comprehensive observability analysis was performed. As a result, feasible design conditions were obtained, which allowed determining the convergence requirements. Finally, the design procedure was formulated as a two-dimensional iterative process. This process boils down to finding a golden solution between two trade-offs, namely, convergence and uncertainty. The final part of the paper showed a numerical example concerning fault estimation of a multi-tank system. The obtained results clearly validate the performance of the proposed estimator within the minimum detectable fault intervals.

The future research direction is focused on extending the proposed scheme towards actuator faults and applying it into reliable and convergence-guaranteed fault-tolerant control.

References

Alessandri, A., Baglietto, M. and Battistelli, G. (2006). Design of state estimators for uncertain linear systems using quadratic boundedness, *Automatica* **42**(3): 497–502.

Blanke, M., Schröder, J., Kinnaert, M., Lunze, J. and Staroswiecki, M. (2006). *Diagnosis and Fault-Tolerant Control*, Springer, Berlin/Heidelberg.

Bounemeur, A., Chemachema, M. and Essounbouli, N. (2018). Indirect adaptive fuzzy fault-tolerant tracking control for MIMO nonlinear systems with actuator and sensor failures, *ISA Transactions* **79**: 45–61.

Boutayeb, M., Darouach, M. and Rafaralahy, H. (2002). Generalized state-space observers for chaotic synchronization and secure communication, *IEEE Transactions on Circuits and Systems I: Fundamental Theory and Applications* **49**(3): 345–349.

Chandra, S., Gupta, M.K. and Tomar, N.K. (2015). Synchronization of Rossler chaotic system for secure communication via descriptor observer design approach, *2015 International Conference on Signal Processing,*

Computing and Control (ISPCC), Waknaghat, India, pp. 120–124.

Chen, F., Niu, J. and Jiang, G. (2018). Nonlinear fault-tolerant control for hypersonic flight vehicle with multi-sensor faults, *IEEE Access* **6**: 25427–25436.

Chen, J. and Patton, R.J. (1999). *Robust Model Based Fault Diagnosis for Dynamic Systems*, Kluwer Academic Publishers, London.

de Oliveira, M., Bernussou, J. and Geromel, J. (1999). A new discrete-time robust stability condition, *Systems and Control Letters* **37**(4): 261–265.

de Oliveira, M.C. and Skelton, R.E. (2007). Stability tests for constrained linear systems, *in* S.O. Reza Moheimani (Ed.), *Perspectives in Robust Control*, Springer, London, pp. 241–257.

Dimassi, H., Lorı, A. and Belghith, S. (2012). A new secured transmission scheme based on chaotic synchronization via smooth adaptive unknown-input observers, *Communications in Nonlinear Science and Numerical Simulation* **17**(9): 3727–3739.

Ding, B. (2010). Constrained robust model predictive control via parameter-dependent dynamic output feedback, *Automatica* **46**(9): 1517–1523.

Gillijns, S. and De Moor, B. (2007). Unbiased minimum-variance input and state estimation for linear discrete-time systems with direct feedthrough, *Automatica* **43**(5): 934–937.

Gupta, M.K., Tomar, N.K., Mishra, V.K. and Bhaumik, S. (2017). Observer design for semilinear descriptor systems with applications to chaos-based secure communication, *International Journal of Applied and Computational Mathematics* **3**: 1313–1324.

Hou, M. and Patton, R.J. (1998). Optimal filtering for systems with unknown inputs, *IEEE Transactions on Automatic Control* **43**(3): 445–449.

Hsieh, C.-S. (2011). Optimal filtering for systems with unknown inputs via the descriptor Kalman filtering method, *Automatica* **47**(10): 2313–2318.

INTECO (2013). *Multitank System—User's Manual*, INTECO, Kraków.

Jung, D. and Frisk, E. (2018). Residual selection for fault detection and isolation using convex optimization, *Automatica* **97**: 143–149.

Kodakkadan, A.R., Pourasghar, M., Puig, V., Olaru, S., Ocampo-Martinez, C. and Reppa, V. (2017). Observer-based sensor fault detectability: About robust positive invariance approach and residual sensitivity, *IFAC-PapersOnLine* **50**(1): 5041–5046.

Kukurowski, N., Mrugalski, M., Pazera, M. and Witczak, M. (2022). Fault-tolerant tracking control for a non-linear twin-rotor system under ellipsoidal bounding, *International Journal of Applied Mathematics and Computer Science* **32**(2): 171–183, DOI: 10.34768/amcs-2022-0013.

Kukurowski, N., Pazera, M. and Witczak, M. (2021a). Fault-tolerant tracking control and remaining useful life estimation for Takagi–Sugeno fuzzy system, *2021 IEEE International Conference on Fuzzy Systems (FUZZ-IEEE), Luxembourg*, pp. 1–7.

Kukurowski, N., Pazera, M. and Witczak, M. (2021b). Fault-tolerant tracking control for a descriptor system under an unknown input disturbances, *Electronics* **10**(18): 2247.

Liu, X., Gao, Z. and Zhang, A. (2018). Robust fault tolerant control for discrete-time dynamic systems with applications to aero engineering systems, *IEEE Access* **6**: 18832–18847.

Mustafa, M.O., Nikolakopoulos, G., Gustafsson, T. and Kominiak, D. (2016). A fault detection scheme based on minimum identified uncertainty bounds violation for broken rotor bars in induction motors, *Control Engineering Practice* **48**: 63–77.

Nasrolahi, S.S. and Abdollahi, F. (2018). Sensor fault detection and recovery in satellite attitude control, *Acta Astronautica* **145**: 275–283.

Patton, R.J. and Chen, J. (1997). Observer-based fault detection and isolation: Robustness and applications, *Control Engineering Practice* **5**(5): 671–682.

Pazera, M., Buciakowski, M. and Witczak, M. (2018). Robust multiple sensor fault-tolerant control for dynamic non-linear systems: Application to the aerodynamical twin-rotor system, *International Journal of Applied Mathematics and Computer Science* **28**(2): 297–308, DOI: 10.2478/amcs-2018-0021.

Pazera, M., Kukurowski, N., Witczak, M. and Buciakowski, M. (2021). A robust Takagi–Sugeno fault diagnostic scheme for remaining useful life estimation, *2021 IEEE International Conference on Fuzzy Systems (FUZZ-IEEE), Luxembourg*, pp. 1–6.

Pazera, M. and Witczak, M. (2019). Towards robust simultaneous actuator and sensor fault estimation for a class of nonlinear systems: Design and comparison, *IEEE Access* **7**: 97143–97158.

Peng, Y., Chen, J. and Ma, Y. (2019). Observer-based estimation of velocity and tire-road friction coefficient for vehicle control systems, *Nonlinear Dynamics* **96**: 363–387.

Pizzi, N., Kofman, E., De Doná, J.A. and Seron, M.M. (2019). Actuator fault tolerant control based on probabilistic ultimate bounds, *ISA Transactions* **84**: 20–30.

Rinaldi, G., Menon, P.P., Edwards, C. and Ferrara, A. (2018). Design and validation of a distributed observer-based estimation scheme for power grids, *IEEE Transactions on Control Systems Technology* **28**(2): 680–687.

Rodrigues, M., Hamdi, H., Theilliol, D., Mechmeche, C. and BenHadj Braiek, N. (2015). Actuator fault estimation based adaptive polytopic observer for a class of LPV descriptor systems, *International Journal of Robust and Nonlinear Control* **25**(5): 673–688.

Rotondo, D., Ponsart, J.-C., Theilliol, D., Nejjari, F. and Puig, V. (2015). A virtual actuator approach for the fault tolerant control of unstable linear systems subject to actuator saturation and fault isolation delay, *Annual Reviews in Control* **39**: 68–80.

Samada, S.E., Puig, V. and Nejjari, F. (2022). Robust fault detection using zonotopic parameter estimation, *IFAC-PapersOnLine* **55**(6): 157–162.

Skelton, R., Iwasaki, T. and Grigoriadis, D. (1997). *A Unified Algebraic Approach to Control Design*, CRC Press, London.

Tan, J., Olaru, S., Roman, M., Xu, F. and Liang, B. (2019). Invariant set-based analysis of minimal detectable fault for discrete-time LPV systems with bounded uncertainties, *IEEE Access* **7**: 152564–152575.

Tan, J., Zheng, H., Meng, D., Yuan, B., Wang, X. and Liang, B. (2023). Confidence set-based analysis of minimal detectable fault under hybrid Gaussian and bounded uncertainties, *Automatica* **155**: 111141.

Wang, H., Han, Z., Zhang, W. and Xie, Q. (2009). Chaotic synchronization and secure communication based on descriptor observer, *Nonlinear Dynamics* **57**(1–2): 69–73.

Wang, W., Geng, Y., Sun, J., Xu, H. and Sheng, L. (2022). Sensor fault detection and minimum detectable fault analysis for dynamic point-the-bit rotary steerable system, *ISA Transactions* **127**: 108–119.

Wen, P., Li, X., Hou, N. and Mu, S. (2022). Distributed recursive fault estimation with binary encoding schemes over sensor networks, *Systems Science & Control Engineering* **10**(1): 417–427.

Witczak, M. (2007). *Modelling and Estimation Strategies for Fault Diagnosis of Non-Linear Systems: From Analytical to Soft Computing Approaches*, Springer, Berlin.

Witczak, M. (2014). *Fault Diagnosis and Fault-Tolerant Control Strategies for Non-Linear Systems*, Lectures Notes in Electrical Engineering, Vol. 266, Springer, Heidelberg.

Witczak, M., Pazera, M., Matysiak, R. and Aubrun, C. (2022). A note on a minimum detectable actuator fault of dynamic systems under ellipsoidal bounding, *26th International Conference on Methods and Models in Automation and Robotics (MMAR), Międzyzdroje, Poland*, pp. 324–329.

Witczak, M., Seybold, L., Bulach, E. and Maucher, N. (2023). *Modern IoT Onboarding Platforms for Advanced Applications: A Practitioner's Guide to KIS.ME*, Springer, Berlin/Heidelberg.

Xu, F. (2022). Minimal detectable and isolable faults of active fault diagnosis, *IEEE Transactions on Automatic Control* **68**(2): 1138–1145.

Yang, J., Zhu, F., Wang, X. and Bu, X. (2015). Robust sliding-mode observer-based sensor fault estimation, actuator fault detection and isolation for uncertain nonlinear systems, *International Journal of Control, Automation and Systems* **13**(5): 1037–1046.

Ye, D., Park, J. and Fan, Q. (2016). Adaptive robust actuator fault compensation for linear systems using a novel fault estimation mechanism, *International Journal of Robust and Nonlinear Control* **26**(8): 1597–1614.

Zemouche, A. and Boutayeb, M. (2013). On LMI conditions to design observers for Lipschitz nonlinear systems, *Automatica* **49**(2): 585–591.

Zemouche, A., Boutayeb, M. and Iulia Bara, G. (2008). Observer for a class of Lipschitz systems with extension to $\mathcal{H}_\infty$ performance analysis, *Systems and Control Letters* **57**(1): 18–27.

Zhang, K., Jiang, B., Shi, P. and Cocquempot, V. (2018). *Observer-based Fault Estimation Techniques*, Springer, Berlin/Heidelberg.

Zhang, Y. and Jiang, J. (2008). Bibliographical review on reconfigurable fault-tolerant control systems, *Annual Reviews in Control* **32**(2): 229–252.

Zhirabok, A. and Shumsky, A. (2018). Fault diagnosis in nonlinear hybrid systems, *International Journal of Applied Mathematics and Computer Science* **28**(4): 635–648, DOI: 10.2478/amcs-2018-0049.

Marcin Witczak was born in Poland in 1973, received his MSc degree in electrical engineering from the University of Zielona Góra (Poland), his PhD degree in automatic control and robotics from the Wrocław University of Technology (Poland), and his DSc degree in electrical engineering from the University of Zielona Góra, in 1998, 2002 and 2007, respectively. In 2015 he received a full professorial title. Since then, Marcin Witczak has been a professor of automatic control and robotics at the Institute of Control and Computation Engineering, University of Zielona Góra. His current research interests include computational intelligence, fault detection and isolation (FDI), fault-tolerant control (FTC), as well as experimental design and control theory. Marcin Witczak has published more than 200 papers in international journals and conference proceedings. He is the author of four monographs and 30 book chapters. Since 2015, he has been a member of the Committee on Automatic Control and Robotics of the Polish Academy of Sciences. As of 2018, he is also an associate editor of *ISA Transactions*. ORCID: 0000-0002-0031-0004.

Marcin Pazera was born in Poland in 1990. He received his MSc degree in control engineering and robotics from the University of Zielona Góra (Poland), and his PhD degree in automatic control, electronics and electrical engineering from the same university in 2015 and 2022, respectively. Currently, he is an assistant professor at the Institute of Control and Computation Engineering there. Marcin Pazera has published altogether 52 works in international journals, book chapters and conference proceedings. His present research interests include fault detection and isolation (FDI), fault-tolerant control (FTC) as well as iterative learning control (ILC) and embedded systems. ORCID: 0000-0003-2469-7570.

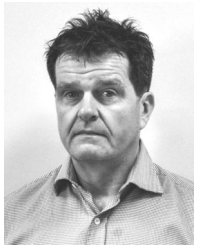

Paweł Majdzik was born in Poland in 1967. He received his MSc degree in electrical engineering from the Wrocław University of Technology and his PhD degree in economics from the Poznań University of Technology, and his DSc degree in computer science from the West Pomeranian University of Technology in Szczecin, in 1992, 1998, and 2023, respectively. He has been with the Institute of Control and Computation Engineering, University of Zielona Góra (Poland), since 1998, currently as an associate professor. His present research interests include design and optimization of DESs, modelling and control of DESs, and fault-tolerant control. Paweł Majdzik has published more than 45 papers in international journals and conference proceedings. He is the author of two monographs. ORCID: 0000-0001-7307-8253.

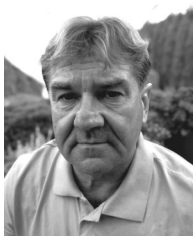

Ryszard Matysiak was born in Poland in 1970. He received his MSc and PhD degrees in physics from Adam Mickiewicz University in Poznań (Poland) in 1994 and 1999, respectively. He has been with the Faculty Mechanical Engineering, University of Zielona Góra (Poland), since 1999, currently as an associate professor. His present research interests include application of statistical analysis in solid state physics and quantum mechanics. Ryszard Matysiak has published more than 28 papers in international journals and conference proceedings. ORCID: 0000-0001-8474-4530.

Received: 8 November 2023
Revised: 4 March 2024
Re-revised: 9 May 2024
Accepted: 10 June 2024